

This article was downloaded by: [University of Waterloo]

On: 15 December 2014, At: 02:26

Publisher: Taylor & Francis

Informa Ltd Registered in England and Wales Registered Number: 1072954 Registered office: Mortimer House, 37-41 Mortimer Street, London W1T 3JH, UK



Engineering Optimization

Publication details, including instructions for authors and subscription information:

<http://www.tandfonline.com/loi/geno20>

Robust design of multiple trailing edge flaps for helicopter vibration reduction: A multi-objective bat algorithm approach

Rajnish Mallick^a, Ranjan Ganguli^a & M. Seetharama Bhat^a

^a Department of Aerospace Engineering, Indian Institute of Science, Bangalore 560012, India

Published online: 08 Oct 2014.



CrossMark

[Click for updates](#)

To cite this article: Rajnish Mallick, Ranjan Ganguli & M. Seetharama Bhat (2014): Robust design of multiple trailing edge flaps for helicopter vibration reduction: A multi-objective bat algorithm approach, *Engineering Optimization*, DOI: [10.1080/0305215X.2014.958734](https://doi.org/10.1080/0305215X.2014.958734)

To link to this article: <http://dx.doi.org/10.1080/0305215X.2014.958734>

PLEASE SCROLL DOWN FOR ARTICLE

Taylor & Francis makes every effort to ensure the accuracy of all the information (the "Content") contained in the publications on our platform. However, Taylor & Francis, our agents, and our licensors make no representations or warranties whatsoever as to the accuracy, completeness, or suitability for any purpose of the Content. Any opinions and views expressed in this publication are the opinions and views of the authors, and are not the views of or endorsed by Taylor & Francis. The accuracy of the Content should not be relied upon and should be independently verified with primary sources of information. Taylor and Francis shall not be liable for any losses, actions, claims, proceedings, demands, costs, expenses, damages, and other liabilities whatsoever or howsoever caused arising directly or indirectly in connection with, in relation to or arising out of the use of the Content.

This article may be used for research, teaching, and private study purposes. Any substantial or systematic reproduction, redistribution, reselling, loan, sub-licensing, systematic supply, or distribution in any form to anyone is expressly forbidden. Terms &

Conditions of access and use can be found at <http://www.tandfonline.com/page/terms-and-conditions>

Robust design of multiple trailing edge flaps for helicopter vibration reduction: A multi-objective bat algorithm approach

Rajnish Mallick*, Ranjan Ganguli and M. Seetharama Bhat

Department of Aerospace Engineering, Indian Institute of Science, Bangalore 560012, India

(Received 27 May 2014; accepted 1 August 2014)

The objective of this study is to determine an optimal trailing edge flap configuration and flap location to achieve minimum hub vibration levels and flap actuation power simultaneously. An aeroelastic analysis of a soft in-plane four-bladed rotor is performed in conjunction with optimal control. A second-order polynomial response surface based on an orthogonal array (OA) with 3-level design describes both the objectives adequately. Two new orthogonal arrays called MGB2P-OA and MGB4P-OA are proposed to generate nonlinear response surfaces with all interaction terms for two and four parameters, respectively. A multi-objective bat algorithm (MOBA) approach is used to obtain the optimal design point for the mutually conflicting objectives. MOBA is a recently developed nature-inspired metaheuristic optimization algorithm that is based on the echolocation behaviour of bats. It is found that MOBA inspired Pareto optimal trailing edge flap design reduces vibration levels by 73% and flap actuation power by 27% in comparison with the baseline design.

Keywords: helicopter vibration; trailing edge flap; multi-objective bat algorithm; response surface; Pareto optimal design

1. Introduction

The helicopter is a versatile vehicle because of its unique capabilities, such as hover, forward and backward manoeuvres, and vertical take-off and landing, which makes it an inevitable machine of choice for defence and civilian operations. The helicopter rotor is a complex dynamical system which experiences asymmetric aerodynamic loading over the rotor disc during forward flight. This asymmetry in lift induces severe vibrations in the rotor system which is usually rich in harmonic content (Loewy, 1984). High vibration levels lead to crew and passenger discomfort, affect avionics reliability, decrease the fatigue life of various structural components and hence lead to an increase in maintenance costs. The helicopter rotor system is also an efficient mechanical filter that filters out all the forces and moments and only allows frequency content that is an integer multiple of the number of blades (or the blade passing frequency, $N_b\Omega$). Here, N_b represents the number of rotor blades and Ω is the rotor rotational speed. In the past, a considerable effort has been expended on vibration suppression research using passive vibration control devices such as vibration isolators or vibration absorbers. Passive devices demonstrate vibration alleviation but possess significant drawbacks as they incur a large weight penalty, increase drag

*Corresponding author. Email: rajnish@aero.iisc.ernet.in

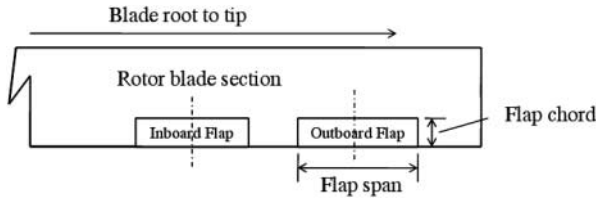


Figure 1. Schematic of rotor blade section with dual flaps.

forces and also their performance degrades from the tuned flight condition (Pearson, Goodall, and Lyndon, 1994).

With the advent of smart materials, active vibration control techniques have caught the attention of researchers (Friedmann and Millott, 1995). In the last two decades, various active approaches were tested numerically (Milgram, Chopra, and Straub, 1998; Cesnik *et al.*, 2004; Lim and Lee, 2009) and experimentally (Noboru *et al.*, 2007; Konstanzer *et al.*, 2008; Sinapius *et al.*, 2014). Piezo actuated active control flap (ACF) methods have emerged as the best potential candidates to alleviate helicopter vibration (Konstanzer *et al.*, 2008). Figure 1 shows a schematic of the rotor blade section with dual trailing edge flaps. Multiple on-blade plain trailing edge flaps (TEFs) are capable of achieving better vibration reduction in comparison to a single TEF. Most of the studies available in the literature use parametric studies to find the best design of trailing edge flaps (Shen and Chopra, 2004). Although active methods are promising, they suffer from high cost and have reliability issues.

Several researchers have tried to address helicopter vibration problems by designing a low vibration rotor using optimization techniques (Chattopadhyay, 1992). Various design variables such as blade mass, stiffness distribution, and advanced blade geometry were studied thoroughly to minimize the vibratory hub loads. A critical review of the use of optimization in helicopter engineering was presented by Ganguli (2004). The integration of optimization algorithms with computationally intensive simulation codes often used in helicopter engineering poses an even greater challenge as it leads to high computational costs. This problem can be resolved by the use of inexpensive surrogate models (metamodels), which can replace the expensive computer analysis codes.

Metamodelling techniques are widely used in multidisciplinary design optimization problems (Sobiesczanski-Sobieski and Haftka, 1997; Simpson *et al.*, 2001; Murugan, Ganguli, and Harursampath, 2012). The response surface method (RSM) is one such metamodelling technique which is widely used in various structural optimization problems (Ganguli, 2002; Bhadra and Ganguli, 2006). The response surface method gives global approximations in contrast to Taylor series which yield only local approximations. Myers and Montgomery have presented an excellent introduction to RSM (Myers, Montgomery, and Anderson-Cook, 2011). RSM is a powerful tool for constructing metamodels for helicopter optimization problems (Viswamurthy and Ganguli, 2007; Glaz *et al.*, 2009). A successful demonstration of the decoupling of a complex structural design problem and the optimization problem was shown using response surfaces for helicopter optimization by Ganguli (2002). Essentially, response surfaces are polynomial approximations to the design analysis problem. Although the computational cost is reduced significantly by using RSM metamodels, nevertheless there is one disadvantage with the response surface method, based on the design of experiments (DOEs). As the number of design variables increases, the computational cost for RSM goes up exponentially. This problem can be ameliorated by the use of orthogonal arrays (OAs).

Orthogonal arrays are simple fractional factorial designs and are used widely in higher dimensional problems for sparse experimental trials. OAs have been extensively used for quality control and parametric optimization. Some researchers have used OAs in conjunction with RSM

to construct response surfaces for optimization studies ([Bhadra and Ganguli, 2006](#); [Mallick, Ganguli, and Bhat, 2013](#)). Hu and Rao developed a robust design method for horizontal axis wind turbines using OAs ([Hu and Rao, 2011](#)).

Most practical engineering problems pose greater challenges for designers because they have multiple objectives that are mutually conflicting in nature ([Geem, 2009](#); [Wilke, 2013](#)). Helicopter design using optimization is a complex and computationally expensive task because of the inherited nonlinearity and contradictory objective functions ([Rao, Dhingra, and Miura, 1990](#)). Global optimizers such as evolutionary algorithms offer superior techniques for addressing the problem at hand ([Crossley, Wells, and Laananen, 1995](#)). Recently, Yang has proposed a bat intelligence inspired metaheuristic algorithm ([Yang, 2011a](#)). It has been shown that the bat algorithm can find global optimal solutions for complex real time optimization problems in a more efficient way than other evolutionary algorithms available in the literature ([Yang, 2011a](#); [Hasançebi, Teke, and Pekcan, 2013](#)). In the research presented herein, the authors present a multi-objective framework for the bat algorithm in the context of multi-objective optimization to find the best trade-off design for multiple trailing edge flaps.

2. Helicopter aeroelastic analysis

A nonlinear model of several elastic rotor blades is used to represent the helicopter. Each rotor blade undergoes flap bending, lag bending, elastic twist, and axial displacement. The formulation is based on the generalized Hamilton's principle applicable to non-conservative systems, *i.e.*

$$\int_{\psi_1}^{\psi_2} (\delta U - \delta T - \delta W) d\psi = 0. \quad (1)$$

Here, δU , δT and δW are the virtual strain energy, virtual kinetic energy and virtual work done, respectively. Finite element methodology is used to discretize the governing equations of motion. Each blade is discretized into 10 spatial elements, with 15 degrees of freedom each. These degrees of freedom are shared over five nodes in each element (two boundary nodes and three internal nodes) ([Bir et al., 1992](#)). The aerodynamic forces and moments acting on the blade section are calculated under high speed forward flight ($\mu = 0.3$). The unsteady aerodynamic model by [Hariharan and Leishman \(1996\)](#) is used to predict the air loads due to rotor blade motion and trailing edge flap deflections. The resulting nonlinear ODEs in time are transformed into the normal mode space and solved for the steady-state blade response using the finite element in time procedure ([Ganguli, 2002](#)). The key finite element equation after normal mode transformation is

$$\bar{\mathbf{M}}\ddot{\mathbf{p}}_b(\psi) + \bar{\mathbf{C}}\dot{\mathbf{p}}_b(\psi) + \bar{\mathbf{K}}\mathbf{p}_b(\psi) - \bar{\mathbf{F}}(\mathbf{p}_b, \psi) = 0, \quad (2)$$

where $\bar{\mathbf{M}} = \Phi^T \mathbf{M}_b \Phi$, $\bar{\mathbf{C}} = \Phi^T \mathbf{C}_b \Phi$, $\bar{\mathbf{K}} = \Phi^T \mathbf{K}_b \Phi$, and $\bar{\mathbf{F}} = \Phi^T \mathbf{F}_b$ represent the modal mass, the damping and stiffness matrices, and the load vector, respectively. Also, \mathbf{p}_b represents the blade response in modal coordinates and \mathbf{M}_b , \mathbf{C}_b , \mathbf{K}_b , and \mathbf{F}_b are the finite element mass, the damping and stiffness matrices, and the force vector, respectively. The blade azimuth angle is denoted by ψ . Once the steady state blade response is determined, the blade root loads are calculated using the force summation method followed by the computation of the loads acting at the rotor hub by summing the contributions of individual blades. A coupled trim procedure is followed to find the blade response, pilot input control angles, and orientation of the vehicle, simultaneously. For a helicopter rotor with N_b identical blades, $N_b\Omega$ is the dominant component of the hub vibratory loads, which is transferred to the fuselage ([Ganguli, 2002](#)). In this investigation, the aim is to obtain an optimal trailing edge flap configuration which will reduce this dominant $N_b\Omega$ load by oscillating the trailing edge flap using a control law.

3. Control algorithm

Research shows that, for an N_b bladed rotor system, the trailing edge flaps are deflected at $(N_b - 1)/\text{rev}$, N_b/rev and $(N_b + 1)/\text{rev}$ harmonics of the rotor's rotational speed. Here, 'rev' implies per revolution (or $\psi = 0^\circ$ to $\psi = 360^\circ$). A careful phasing of the trailing edge flap motion generates new unsteady aerodynamic loads which cancel the original oscillatory aerodynamic loads. A multi-harmonic control law is used for the flap motion ($\delta_i(\psi)$),

$$\delta_i(\psi) = \delta_i^{3c} \cos(3\psi) + \delta_i^{3s} \sin(3\psi) + \delta_i^{4c} \cos(4\psi) + \delta_i^{4s} \sin(4\psi) + \delta_i^{5c} \cos(5\psi) + \delta_i^{5s} \sin(5\psi). \quad (3)$$

An optimal control algorithm is used to obtain the six unknown flap harmonics in the above control law (Johnson, 1982; Mallick, Ganguli, and Bhat, 2014). The algorithm is based on the minimization of a scalar quadratic objective function comprising 4/rev hub loads (\mathbf{Z}) and flap control harmonics (\mathbf{u}),

$$J_v = \mathbf{Z}^T \mathbf{W}_z \mathbf{Z} + \mathbf{u}^T \mathbf{W}_u \mathbf{u}. \quad (4)$$

Hub vibration levels are represented by the first term in the above equation. The weighting matrix \mathbf{W}_u is adjusted to ensure the peak deflection of both flaps are within achievable limits using the current state-of-the-art smart materials. The hub load vector \mathbf{Z} contains three hub forces and three hub moments, and \mathbf{u} is the control input vector. The weighting matrix \mathbf{W}_z is usually a diagonal matrix which can be suitably modified to make the controller reduce either the hub shears or moments. In this study, a constant weighting matrix is used by setting the parameter $\alpha = 0.5$, which gives equal importance to either hub load.

$$\mathbf{Z} = [F_{xH}^{4P} \ F_{yH}^{4P} \ F_{zH}^{4P} \ M_{xH}^{4P} \ M_{yH}^{4P} \ M_{zH}^{4P}]^T \quad (5)$$

$$\mathbf{u}_i = [\delta_i^{3c} \ \delta_i^{3s} \ \delta_i^{4c} \ \delta_i^{4s} \ \delta_i^{5c} \ \delta_i^{5s}]^T \quad (6)$$

$$\mathbf{W}_z = (1 - \sum_{i=1}^{N_f} \beta_i) \begin{bmatrix} \alpha \mathbf{I}_{3 \times 3} & \mathbf{0}_{3 \times 3} \\ \mathbf{0}_{3 \times 3} & 1 - \alpha \mathbf{I}_{3 \times 3} \end{bmatrix} \quad (7)$$

$$\sum_{i=1}^{N_f} \beta_i \leq 1. \quad (8)$$

A global controller is used to determine the optimal control input. The hub load vector \mathbf{Z} is related to the control inputs using a transfer matrix. Linearizing the system about the control inputs using Taylor's series expansion gives

$$\mathbf{Z} = \mathbf{Z}_0 + \mathbf{T} \mathbf{u}. \quad (9)$$

The forward finite difference method is used to obtain the transfer matrix \mathbf{T} by perturbing the control harmonics individually around zero control inputs. Equation (9) is substituted into Equation (4), followed by the optimality condition,

$$\frac{\partial J_v}{\partial \mathbf{u}} = 0. \quad (10)$$

Thus the optimal controller becomes

$$\mathbf{u} = \mathbf{C} \mathbf{Z}_0 \quad (11)$$

$$\mathbf{C} = -\mathbf{D} \mathbf{T}^T \mathbf{W}_z \quad (12)$$

$$\mathbf{D} = (\mathbf{T}^T \mathbf{W}_z \mathbf{T} + \mathbf{W}_u)^{-1}. \quad (13)$$

The power required by the actuation system (J_p) is obtained by integrating the product of the hinge moment and flap deflection rate over the azimuth. Although the instantaneous power required at the flap hinge, $-M_h\dot{\delta}$, may be negative over some portions of the azimuth, it is assumed that the actuator is unable to transfer the power back to its power supply, hence the mean actuation power for an N_b bladed rotor system with N_f flaps located on the blade is given as (Milgram, Chopra, and Straub, 1998)

$$J_p = N_b/2\pi \sum_{i=1}^{N_f} \int_0^{2\pi} \max(-M_{hi}\dot{\delta}_i, 0) d\psi. \quad (14)$$

In the present study, the aerodynamic contribution to the hinge moment due to harmonic flap motion is captured using compressible unsteady aerodynamic effects through indicial function representation (Hariharan and Leishman, 1996). The inertial contribution to the trailing edge flap hinge moment is calculated as

$$M_h = - \int \int (\vec{\rho}_h \times \vec{a}) \cdot \hat{i}_h dm_f. \quad (15)$$

Here, dm_f is an elemental mass on the active trailing edge flap in the transverse plane ($y - z$), $\vec{\rho}_h$ is a position vector in the ‘h’ (hinge) coordinate system, and \vec{a} is the acceleration of the elemental mass.

4. Optimization problem

The objective of this investigation is to search for an optimal design configuration and locations for dual trailing edge flaps. The design variables in this study are flap chord and flap length for the 2-parameter case, and flap chord, flap length, and flap locations for the 4-parameter case. A robust optimization technique is used to achieve the objective of minimum vibration levels, simultaneously reducing the power required for the actuation of flaps. Helicopter vibration alleviation using active trailing edge flaps is the subject of investigation in this study. However, the available power required for flap actuation J_p is limited in flight and should be minimum. Therefore, both vibration level J_v and required flap actuation power J_p are chosen as the design objectives in this study. Flaps are located at their baseline locations for the vibration reduction objective function in the 2-parameter case (Viswamurthy and Ganguli, 2007). Midpoint of inboard and outboard flaps are located at 67% R and 79% R from the blade root, respectively in search of optimal flap dimensions. However, flap locations are also considered as variables in the 4-parameter case to find optimal flap locations and dimensions. The values of J_v and J_p are normalized with respect to the respective baseline design point. These normalized values are denoted by F_v and F_p , respectively. The superscripts ‘2param’ and ‘4param’ are used to denote the variables associated with the 2-parameter and 4-parameter problems, respectively. The optimization problem for four parameters is formulated as follows:

$$\text{Minimize } \{F_v, F_p\} \quad (16)$$

$$\text{subject to: } x_{1,\text{lower}} \leq x_1 \leq x_{1,\text{upper}} \quad (17)$$

$$x_{2,\text{lower}} \leq x_2 \leq x_{2,\text{upper}} \quad (18)$$

$$x_{3,\text{lower}} \leq x_3 \leq x_{3,\text{upper}} \quad (19)$$

$$x_{4,\text{lower}} \leq x_4 \leq x_{4,\text{upper}}. \quad (20)$$

Here x_1 , x_2 , x_3 , and x_4 are the design variables, representing inboard location, outboard location, flap length, and flap chord, respectively. The objective functions are of conflicting nature for the same choice of design variables, which implies that to attain high levels of vibration reduction requires large flap actuation power. This kind of optimization problems falls under the category of multi-objective design optimization. An optimization solution is said to be Pareto optimal if it is impossible to minimize one objective without increasing the other objective.

A response surface method (RSM) is used to obtain surrogate models of the objective function in terms of second-order polynomials. The optimization problem is decoupled from the expensive aeroelastic analysis using the RSM technique. Henceforth, these second-order polynomial approximations will serve as the objective functions which will be analysed for Pareto optimal design points using computationally efficient evolutionary optimization algorithms such as the multi-objective bat algorithm (MOBA).

5. Response surface methods

Response surface methods (RSMs) are a collection of statistical and mathematical techniques which are used for improving and optimizing products and processes. RSMs generate a functional relation between an output variable and a set of input variables (independent variables) ([Myers, Montgomery, and Anderson-Cook, 2011](#); [Ganguli, 2012](#)),

$$y = f(x) + \epsilon. \quad (21)$$

In the RSM approach, f is an unknown function and the error ϵ is treated as a statistical error, with zero nominal distribution, zero mean, and zero variance. Here, the relationship between input variables and output (response) is obtained using a low number of design experiments using orthogonal arrays. Response surfaces are generally approximated with second-order polynomials, as they capture the curvature and interaction effects along with the slope. A second-order response surface is obtained by a polynomial multiple regression technique to approximate the objective functions. For instance, a general second-order polynomial response surface is

$$y(x_i) = \beta_0 + \sum_{i=1}^k \beta_i x_i + \sum_{i=1}^k \beta_{ii} x_i^2 + \sum_{i < j}^k \sum_j^k \beta_{ij} x_i x_j + \epsilon. \quad (22)$$

A second-order polynomial response surface y for two and four design variables is modelled as

$$y(x_1, x_2) = \beta_0 + \beta_1 x_1 + \beta_2 x_2 + \beta_{11} x_1^2 + \beta_{22} x_2^2 + \beta_{12} x_1 x_2 + \epsilon \quad (23)$$

$$\begin{aligned} y(x_1, x_2, x_3, x_4) = & \beta_0 + \beta_1 x_1 + \beta_2 x_2 + \beta_3 x_3 + \beta_4 x_4 + \beta_{11} x_1^2 + \beta_{22} x_2^2 \\ & + \beta_{33} x_3^2 + \beta_{44} x_4^2 + \beta_{12} x_1 x_2 + \beta_{13} x_1 x_3 + \beta_{14} x_1 x_4 \\ & + \beta_{23} x_2 x_3 + \beta_{24} x_2 x_4 + \beta_{34} x_3 x_4 + \epsilon. \end{aligned} \quad (24)$$

Regression analysis is used to obtain the regression coefficients β_0 , β_i , β_{ii} , and β_{ij} . The method of least squares is invoked to estimate the regression coefficients, which minimizes the sum of the squares of the deviation of the predicted values $\hat{y}(x)$ from the actual $y(x)$. Regression coefficients are obtained from Equations (23) and (24) by writing it in matrix form, $\mathbf{y} = \mathbf{X}\beta + \epsilon$. Both response \mathbf{y} and error ϵ are n -dimensional vectors and β is a k -dimensional vector of regression coefficients. Here, k is the number of design points and \mathbf{X} is the matrix of sample data

points with dimension $n \times k$. Regression coefficients are obtained by minimizing the least square error obtained using the following relation:

$$L = \sum_{i=1}^n \epsilon_i^2 = \epsilon^T \epsilon = (\mathbf{y} - \mathbf{X}\beta)^T(\mathbf{y} - \mathbf{X}\beta). \quad (25)$$

Therefore, with the best estimate of the regression coefficients as $\hat{\beta} = (\mathbf{X}^T \mathbf{X})^{-1} \mathbf{X}^T \mathbf{y}$, the model has been fitted for the response surfaces as

$$\hat{\mathbf{y}}(x) = \mathbf{X}\hat{\beta}. \quad (26)$$

6. Orthogonal arrays

Orthogonal arrays (OAs) provide a systematic approach to perform numerical experiments with only a fraction of the design points needed for factorial design (Ganguli, 2012; Roy, 2010). In the present research, two new 3-level design orthogonal arrays called MGB2P-OA and MGB4P-OA are proposed for non-singular matrix evaluation to create second-order polynomial response surfaces with all interaction terms for two and four parameters, respectively. Fractional factorial experimental design uses only a fraction of the total number of possible combinations to estimate the main effects and interactions. Here, orthogonality means that the factors can be evaluated independently of each other. MGB2P-OA and MGB4P-OA for a 3-level design are shown in Tables 1 and 2. The values $-1, 0$, and 1 in the tables correspond to the three levels of the design variables. Note that the columns corresponding to the design variables in Tables 1 and 2 are orthogonal to each other. In general form, for an orthogonal array,

$$\begin{aligned} \mathbf{X}_{\text{OA}} &= [\mathbf{x}_1, \mathbf{x}_2, \dots, \mathbf{x}_n] \\ \mathbf{x}_i^T \mathbf{x}_j &= 0; i \neq j. \end{aligned} \quad (27)$$

7. Multi-objective bat algorithm

A new metaheuristic search algorithm called the multi-objective bat algorithm (MOBA) has been developed recently (Yang, 2011a). It has been shown that the MOBA algorithm is highly efficient

Table 1. A 3-level MGB2P-OA orthogonal array for two parameters.

Sample point	Design variables	
	x_1	x_2
1	1	1
2	1	-1
3	-1	-1
4	-1	1
5	0	0
6	0	1
7	1	0
8	-1	0
9	0	-1

Table 2. A 3-level MGB4P-OA orthogonal array for four parameters.

Sample point	Design variables			
	x_1	x_2	x_3	x_4
1	-1	-1	-1	-1
2	0	0	0	0
3	1	1	1	1
4	0	0	1	1
5	1	1	-1	-1
6	-1	-1	0	0
7	-1	1	0	1
8	0	-1	1	-1
9	1	0	-1	0
10	1	0	0	-1
11	-1	1	1	0
12	0	-1	-1	1
13	1	-1	1	0
14	-1	0	-1	1
15	0	1	0	-1
16	0	1	-1	0
17	1	-1	0	1
18	-1	0	1	-1

and outperforms already existing algorithms (Yang, 2011b; Yang and Gandomi, 2012; Yang and He, 2013). In this investigation, the MOBA algorithm is employed for multi-objective design optimization of trailing edge flaps for helicopter vibration reduction. The bat algorithm is based on the natural echolocation capability of bats and a brief survey of the bat algorithm is outlined below.

7.1. Echolocation of bats

Bats are quite interesting mammals, with fascinating capabilities of echolocation. They are the only mammals with wings. There are about 996 species of bats and their size varies from tiny bumblebee bats (~ 2 g) to giant bats (~ 1 kg) with a wing span of around 2 m. Among the plethora of bat species, which account for about 20% of all mammal species, microbats (with forearm length of between 2.2 to 11 cm) use echolocation quite extensively (Richardson, 2011). Microbats use a type of sonar system known as echolocation to avoid obstacles, for prey detection, and also to locate their roosting crevices in the pitch-dark. These bats transmit loud pulses of sound and listen to the echo reflected from the surroundings. The pulse variations can be correlated with their hunting methods, which are species dependent. Generally, each pulse has a constant frequency, which is in the region 25 to 150 kHz. Usually, these ultrasonic bursts last for a few thousandths of a second (5 to 20 ms) and microbats transmit about 200 bursts per second (when they are approaching their prey). These short and intense ultrasonic bursts show the fantastic capability for signal processing of bats (Richardson, 2011; Yang, 2011a).

Typically, the speed of sound in air is $v = 340$ m/s. The ultrasonic sound bursts with constant frequency f and wavelength λ are correlated as

$$\lambda = \frac{v}{f}. \quad (28)$$

For the frequency range 25 to 150 kHz, the wavelength λ falls in the range of 2 to 14 mm, and such wavelengths are of the same order as their prey size. Altringham reported that microbats use the time difference between their two ears, the time delay between the emission and

reception of the echo, and the echolocation variation to create a three-dimensional map of the environment (Altringham, Hammond, and McOwat, 1996). It was shown that bats can precisely predict the location and speed of the target and types of prey. Robust optimization algorithms can be formulated towards minimization of an objective, which can be closely associated with the echolocation strategy of microbats.

7.2. Pareto optimal multi-objective bat algorithm

Some idealizations are used to develop the echolocation characteristics in the bat algorithm (Yang, 2011a). Bats fly randomly with velocity v_i and frequency f_{\min} towards location x_i . They search for prey with loudness A_0 and wavelength λ . Bats can adjust the rate and wavelength (frequency) of the emitted pulses according to the target locations such that $r \in [0, 1]$ and $A_0 \in [1, 2]$. Bats wander the ' d '-dimensional search space with velocities v_i and location x_i , as per the following rules:

$$\begin{aligned} f_i &= f_{\min} + (f_{\max} - f_{\min})\beta \\ v_i^t &= v_i^{t-1} + (x_i^t - x_*)f_i \\ x_i^t &= x_i^{t-1} + v_i^t. \end{aligned} \quad (29)$$

Here, $\beta \in [0, 1]$ is a random vector evaluated using a uniform distribution. Here, x_* is the current global best position, which is found after comparing all the solutions among all n bats at time t . Initially, each bat is randomly assigned a frequency obtained from a uniform distribution of $[f_{\min}, f_{\max}]$. Once a solution is selected among the current best solutions, a new solution for an individual bat is generated locally using a random walk:

$$x_{\text{new}} = x_{\text{old}} + \epsilon A^t. \quad (30)$$

Here $\epsilon \in [-1, 1]$ is a random vector and $A^t = \langle A_i^t \rangle$ is the average loudness of all the bats at time step t . The loudness A_i and rate r_i of pulse emission is updated as bats approach towards their prey. Here, $A_0 = 1$ and $A_{\min} = 0$ have been chosen, where A_0 implies that the bat has found its target and stopped emitting any pulses. Thus,

$$\begin{aligned} A_i^{t+1} &= \alpha A_i^t \\ r_i^t &= r_i^0 [1 - \exp(-\gamma t)], \end{aligned} \quad (31)$$

where α and γ are constants. For $\alpha \in [0, 1]$ and $\gamma > 0$, $A_i^t \rightarrow 0$ and $r_i^t \rightarrow r_i$ as $t \rightarrow \infty$.

Multi-objective optimization problems are often more complex than single objective optimization ones. Tradeoff design strategies such as Pareto optimal fronts can be constructed to obtain an optimal compromise design. The Pareto front (PF) of a multi-objective problem can be defined as the set of ‘non-inferior’ or ‘non-dominated’ solutions, such that (Coello Coello, 1999; Deb, 2001; Yang, 2011a)

$$\text{PF} = \{s \in S \mid \nexists s' \in S : s' \prec S\}. \quad (32)$$

Here, ‘non-dominated’ solutions imply that a solution vector $\mathbf{a} = \{a_1, a_2, \dots, a_n\}^T \in \mathcal{A}$ is said to dominate over vector $\mathbf{b} = \{b_1, b_2, \dots, b_n\}^T$ if and only if $a_i \leq b_i \forall i \in \{1, 2, \dots, n\}$ and $\exists i \in \{1, 2, \dots, n\} : a_i < b_i$. This means that no element of \mathbf{a} is greater than the corresponding entry of \mathbf{b} and at least one component is smaller. Therefore, another dominance relation \preceq can be defined as

$$\mathbf{a} \preceq \mathbf{b} \Leftrightarrow \mathbf{a} \prec \mathbf{b} \vee \mathbf{a} = \mathbf{b}. \quad (33)$$

Therefore, an optimal location $x_* \in \mathcal{A}$ is called a non-dominated solution if no solution is found which dominates it (Coello Coello, 1999). Hence, for the predefined search space, the Pareto

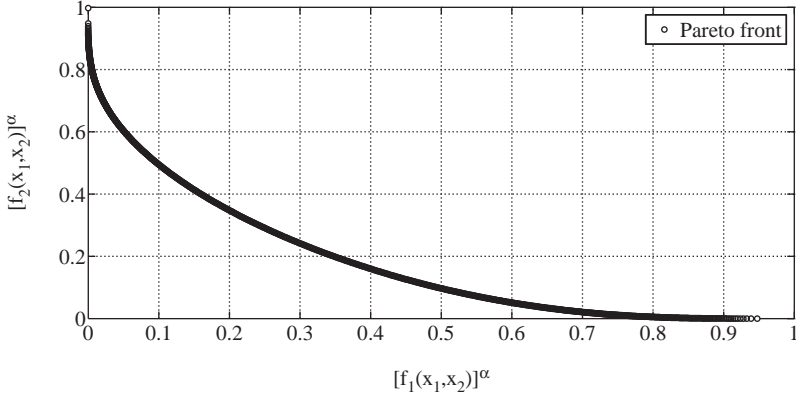


Figure 2. The Pareto front for the Fonseca and Fleming test function.

optimal set PF^* is

$$\text{PF}^* = \{x \in \mathcal{A} \mid \nexists x' \in \mathcal{A} : \mathbf{f}(x') \prec \mathbf{f}(x)\}. \quad (34)$$

Here, $\mathbf{f} = (f_1, f_2, \dots, f_K)$ is a K -dimensional set of functions. The set of K objectives is combined into a single objective using a weighted sum such that

$$f = \sum_{i=1}^K w_i f_i, \quad \sum_{i=1}^K w_i = 1. \quad (35)$$

In this investigation, weights are varied systematically to generate the Pareto front. In this study, the authors have used two objectives, $J_v(F_v)$ and $J_P(F_P)$, to obtain the optimal flap configurations for multiple trailing edge flaps for helicopter vibration reduction.

The MOBA algorithm is implemented on a multi-objective test function and a Pareto front is constructed for demonstration. Here, the bi-objective function due to Fonseca and Fleming is used for the test case to obtain the Pareto front ([Fonseca and Fleming, 1995](#)). The test function is given as

$$\begin{aligned} f_1(x_1, x_2) &= 1 - e^{(-(x_1-1)^2-(x_2+1)^2)} \\ f_2(x_1, x_2) &= 1 - e^{(-(x_1+1)^2-(x_2-1)^2)}, \end{aligned} \quad (36)$$

where, x_1, x_2 are the decision variables and f_1, f_2 are the objective functions in the test function. [Fonseca and Fleming \(1995\)](#) studied the Pareto fronts for the rescaled functions and their influence on the concavity of the trade-off sets. The functions are scaled by a factor $\alpha = 9$. The Pareto front using the MOBA algorithm for a rescaled Fonseca and Fleming test function is shown in Figure 2. This illustrates that the multi-objective bat algorithm accurately generates the Pareto front information for the test case.

8. Results and discussion

In this study, results are obtained for a 4-bladed, soft in-plane, uniform, hingeless rotor similar to the BO105 rotor. Baseline rotor and trailing edge flap properties are shown in Table 3. The move limits of design/decision variables (flap length and flap chord) in physical and coded form are mentioned in Tables 4 and 5, respectively, for the 2-parameter case. Both inboard and outboard

flap chord and span vary from $0.10c$ to $0.20c$ and $4\%R$ to $10\%R$, respectively, in both the 2-parameter and the 4-parameter case. However, in the 4-parameter case, flap locations are also set as variables, along with flap span and chord as decision variables. Table 6 shows the physical and coded values for the 4-parameter case with four design variables. Here, c represents the blade chord and R is the rotor radius. The bounds on the design space are determined by the physical constraints. The largest flap span is chosen as $10\%R$, such that a single actuator should be able to deflect the flap adequately. On the other hand, the lower bound on flap length is selected to ensure enough oscillatory moment generation by the flap to reduce the hub loads.

Table 3. Baseline rotor properties.

Number of blades	4
c/R	0.055
Solidity, σ	0.07
Lock number, γ	5.20
C_T/σ	0.07
Blade pretwist	0.0
Precone, β_p	0.0
$EI_y/m_0\Omega^2 R^4$	0.0108
$EI_z/m_0\Omega^2 R^4$	0.0268
$GJ/m_0\Omega^2 R^4$	0.00615
m_0 (kg/m)	6.46
Ω (rpm)	383
R (m)	4.94

Table 4. J_v at coded and physical values of design variables for two parameters.

Coded values	Length, x_1	-1	0	1
Chord, x_2	Physical values	$4\%R$	$6\%R$	$10\%R$
-1	$0.10c$	5.46E-06	4.12E-06	3.60E-06
-0	$0.15c$	4.99E-06	3.93E-06	3.56E-06
-1	$0.20c$	4.79E-06	3.87E-06	3.55E-06

Table 5. J_P at coded and physical values of design variables for two parameters.

Coded values	Length, x_1	-1	0	1
Chord, x_2	Physical values	$4\%R$	$6\%R$	$10\%R$
-1	$0.10c$	3.98E-08	4.89E-08	5.50E-08
-0	$0.15c$	5.73E-08	6.86E-08	7.70E-08
-1	$0.20c$	7.76E-08	9.28E-08	1.10E-07

Table 6. Coded and physical values of design variables for four parameters.

Coded values	-1	0	1
	Physical values		
Inboard, x_1	$56\%R$	$62\%R$	$68\%R$
Outboard, x_2	$78\%R$	$84\%R$	$90\%R$
Length, x_3	$4\%R$	$6\%R$	$10\%R$
Chord, x_4	$0.10c$	$0.15c$	$0.20c$

8.1. Response surfaces for dual flap configurations

Two new 3-level design orthogonal arrays (MGB2P-OA and MGB4P-OA) are employed to construct second-order polynomial response surfaces F_v and F_P with all interaction terms, to approximate helicopter aeroelastic analysis predictions adequately. The response surfaces for two and four parameters using the least squares method are

$$F_v^{2\text{param}} = 0.9992 - 0.1918x_1 - 0.0412x_2 + 0.0892x_1^2 + 0.0168x_1x_2 + 0.0395x_2^2 \quad (37)$$

$$F_P^{2\text{param}} = 0.9923 + 0.1635x_1 + 0.3317x_2 - 0.0099x_1^2 + 0.0439x_1x_2 + 0.0623x_2^2 \quad (38)$$

$$\begin{aligned} F_v^{4\text{param}} = & 1.0544 - 0.0631x_1 - 0.1197x_2 - 0.2193x_3 - 0.0611x_4 + 0.0854x_1^2 \\ & - 0.0829x_2^2 - 0.0237x_3^2 - 0.0392x_4^2 + 0.0639x_1x_2 + 0.0213x_1x_3 \\ & - 0.0195x_1x_4 - 0.0479x_2x_3 - 0.0480x_2x_4 + 0.0333x_3x_4 \end{aligned} \quad (39)$$

$$\begin{aligned} F_P^{4\text{param}} = & 0.9754 - 0.0568x_1 + 0.1419x_2 + 0.2673x_3 + 0.3383x_4 - 0.0320x_1^2 \\ & - 0.0578x_2^2 + 0.1097x_3^2 + 0.0609x_4^2 + 0.0455x_1x_2 + 0.0019x_1x_3 \\ & + 0.0045x_1x_4 + 0.0931x_2x_3 + 0.0208x_2x_4 + 0.0878x_3x_4. \end{aligned} \quad (40)$$

Tables 7–10 show a comparison of the response surface prediction and an aeroelastic analysis using MGB2P-OA and MGB4P-OA for the F_v and F_P responses, respectively. It is interesting to note that the maximum variation between the surrogate prediction and the aeroelastic analysis is around 6% for F_v and 4% for F_P for both OAs. The response surfaces for F_v and F_P for two parameters, flap length, and flap chord are shown in Figures 3 and 4, respectively.

Figure 3 illustrates that the flap length is the dominant parameter to minimize $F_v^{2\text{param}}$. This is also evident from the expression for the objective function in Equation (37) for $F_v^{2\text{param}}$, as the coefficient of the flap length parameter x_1 is one order of magnitude higher than the flap chord parameter x_2 . Figure 4 shows the variation of the response surface $F_P^{2\text{param}}$. In this case, the variation is controlled by the flap chord ratio.

In the 4-parameter case, it is apparent from the vibration objective $F_v^{4\text{param}}$ that the outboard flap location x_2 has a more pronounced effect on the response than the inboard flap position x_1 . However, the authors have found that the flap length x_3 has a prevalent effect on the response function in comparison to the flap chord x_4 , which is also in agreement with the authors' findings for the 2-parameter case. For the response $F_P^{4\text{param}}$, again the outboard flap location contributes more than the inboard flap, while the flap chord takes precedence over the flap length for flap

Table 7. Comparison between predicted response and aeroelastic analysis for F_v using MGB2P-OA.

Sample point	Coded values		RSM prediction, $F_v^{2\text{param}}$	Analysis prediction, $F_v^{2\text{param}}$	Error (%)
	x_1	x_2			
1	1	1	0.9021	0.9118	1.07
2	1	-1	0.9151	0.9605	4.96
3	-1	-1	1.3877	1.3776	-0.73
4	-1	1	1.2166	1.2618	3.71
5	0	0	1.0000	0.9992	-0.08
6	0	1	0.9842	0.9976	1.36
7	1	0	0.9062	0.8966	-1.06
8	-1	0	1.2698	1.2802	0.82
9	0	-1	1.0470	1.0799	3.14

Table 8. Comparison between predicted response and aeroelastic analysis for F_P using MGB2P-OA.

Sample point	Coded values		RSM prediction, $F_P^{2\text{param}}$	Analysis prediction, $F_P^{2\text{param}}$	Error (%)
	x_1	x_2			
1	1	1	1.6016	1.5838	-1.11
2	1	-1	0.8014	0.8326	3.90
3	-1	-1	0.5794	0.5934	2.41
4	-1	1	1.1303	1.169	3.43
5	0	0	1.0000	0.9923	-0.77
6	0	1	1.3519	1.3863	2.54
7	1	0	1.1224	1.1459	2.09
8	-1	0	0.8346	0.8188	-1.89
9	0	-1	0.7128	0.7229	1.42

Table 9. Comparison between predicted response and aeroelastic analysis for F_v using MGB4P-OA.

Sample point	Coded values				RSM prediction, $F_v^{4\text{param}}$	Analysis prediction, $F_v^{4\text{param}}$	% Error
	x_1	x_2	x_3	x_4			
1	-1	-1	-1	-1	1.4562	1.4603	0.3
2	0	0	0	0	1.0000	1.0544	5.4
3	1	1	1	1	0.5296	0.5339	0.8
4	0	0	1	1	0.7653	0.7444	-2.7
5	1	1	-1	-1	1.2534	1.2829	2.4
6	-1	-1	0	0	1.3245	1.3036	-1.6
7	-1	1	0	1	0.7996	0.8076	1.0
8	0	-1	1	-1	0.8577	0.8367	-2.5
9	1	0	-1	0	1.3147	1.2510	-4.8
10	1	0	0	-1	1.0961	1.1181	2.0
11	-1	1	1	0	0.6237	0.6242	0.1
12	0	-1	-1	1	1.1239	1.1533	2.6
13	1	-1	1	0	0.8678	0.8758	0.9
14	-1	0	-1	1	1.3267	1.3057	-1.6
15	0	1	0	-1	0.9853	0.9217	-6.5
16	0	1	-1	0	1.0733	1.0953	2.0
17	1	-1	0	1	0.9772	0.9778	0.1
18	-1	0	1	-1	0.8783	0.9077	3.3

actuation power requirements, as is also apparent from the order of magnitudes of the variables in the respective expressions.

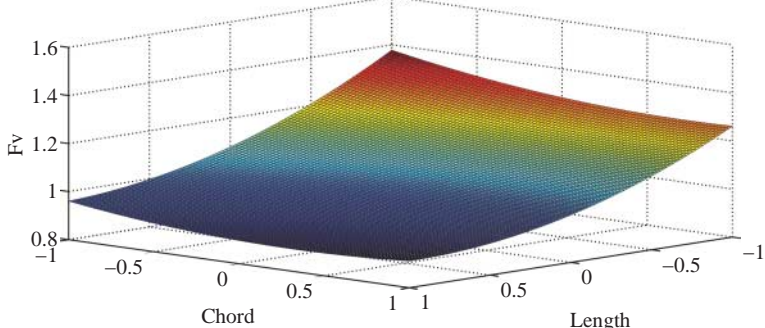
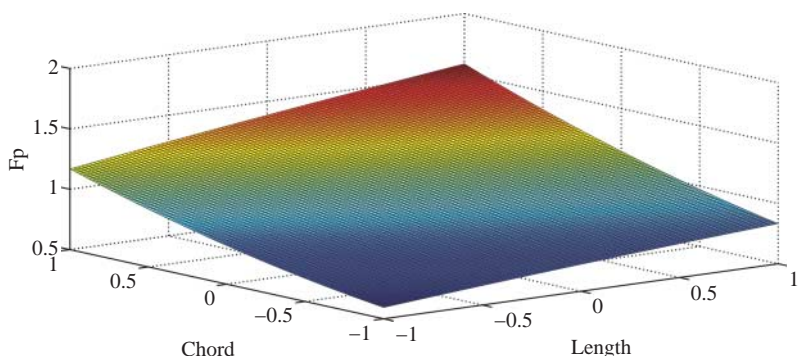
Since both the objectives possess conflicting behaviour towards the decision variables in both cases, a multi-objective Pareto optimal design approach is used to obtain the optimal flap configuration.

8.2. Multi-objective Pareto optimal design

A newly developed multi-objective bat algorithm (MOBA) is implemented to construct the Pareto front for obtaining global optimal solutions. In this research, the authors have considered a bat population of $n = 10$, an initial loudness of $A_i^0 = 0.25$, and an initial emission rate of $r_i^0 = 0.5$, while the loudness ratio α and pulse reduction rate γ are set as 0.9. MOBA based optimization is found to be computationally efficient for global search in the design space. It requires less than 3 seconds for 100 iterations with a population size of 10 bats on a normal computer for 2 parameters and 16 seconds for 4 parameters using MGB2P-OA and MGB4P-OA

Table 10. Comparison between predicted response and aeroelastic analysis for F_P using MGB4P-OA.

Sample point	Coded values				RSM prediction, $F_P^{4\text{param}}$	Analysis prediction, $F_P^{4\text{param}}$	% Error
	x_1	x_2	x_3	x_4			
1	-1	-1	-1	-1	0.6209	0.6191	-0.3
2	0	0	0	0	1.0000	0.9754	-2.5
3	1	1	1	1	2.0024	2.0005	-0.1
4	0	0	1	1	1.8299	1.8394	0.5
5	1	1	-1	-1	0.5620	0.5487	-2.4
6	-1	-1	0	0	0.8365	0.8460	1.1
7	-1	1	0	1	1.4372	1.4543	1.2
8	0	-1	1	-1	0.7296	0.7152	-2.0
9	1	0	-1	0	0.7049	0.7271	3.1
10	1	0	0	-1	0.6079	0.6047	-0.5
11	-1	1	1	0	1.5277	1.5070	-1.4
12	0	-1	-1	1	0.9910	1.0018	1.1
13	1	-1	1	0	0.9101	0.9272	1.9
14	-1	0	-1	1	1.1657	1.1514	-1.2
15	0	1	0	-1	0.7390	0.7613	3.0
16	0	1	-1	0	0.8120	0.8088	-0.4
17	1	-1	0	1	1.0450	1.0243	-2.0
18	-1	0	1	-1	1.0038	1.0146	1.1

Figure 3. Variation in F_v for trailing edge flap length and chord dimensions in design space for two parameters.Figure 4. Variation in F_P for trailing edge flap length and chord dimensions in design space for two parameters.

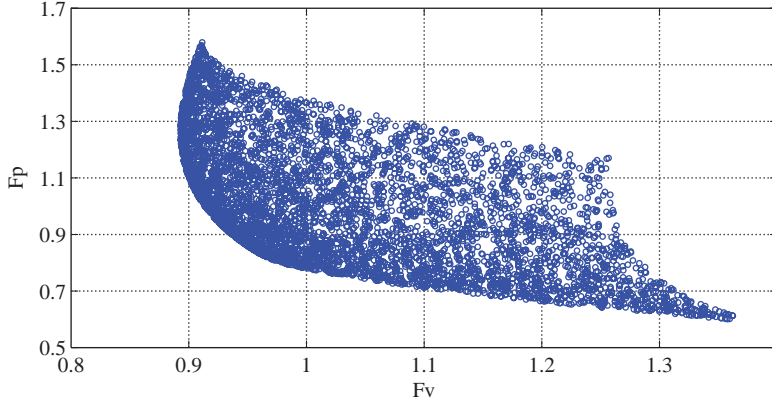


Figure 5. Objective space for the dual flap configuration with two parameters.

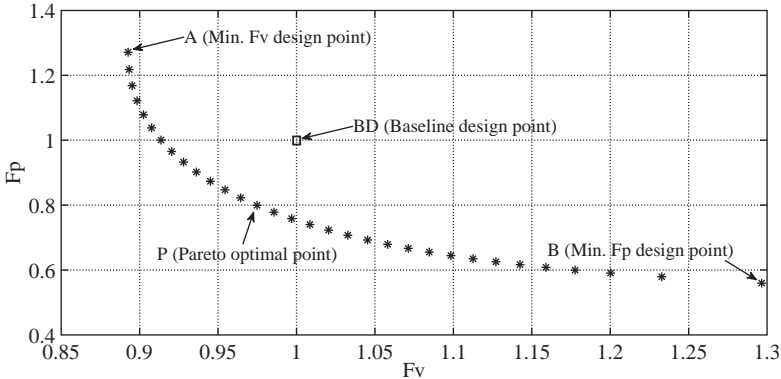


Figure 6. Pareto curve for the dual flap configuration with two parameters.

orthogonal arrays. On the other hand, the aeroelastic analysis code takes around 1080 seconds and 2160 seconds to run the simulation for 9 and 18 DOEs on a Linux machine, respectively. Figure 5 depicts the objective space for 2-parameter flap length and flap chord. Figure 6 shows the Pareto front obtained using MOBA with mutually conflicting objectives for the 2-parameter case. It is evident from Figure 6 that there are two extreme points of interest, point A and point B. Design point A represents a flap configuration which yields minimum vibration levels, while the flap design inspired from design point B requires minimum flap actuation power. Here, the baseline design point BD represents $F_v = F_p = 1$.

The flap configuration advised by design point A reduces hub loads by 72% from the baseline (w/o flaps) at a cost of 60% more flap power requirement in comparison to baseline design BD. On the other hand, minimum $F_p^{2\text{param}}$ can be achieved with the design point B configuration, which yields around 58% reduction in hubloads and requires 42% less power to actuate the flaps relative to the the baseline design BD. Due to the conflicting nature of the objectives, a Pareto optimal point P is selected from the Pareto curve. Design configuration P suppresses vibratory loads by 71% from the baseline (w/o flaps), which is also around 3% more than the baseline design point BD and it requires 20% less flap actuation power. From the MOBA algorithm, it is observed that the Pareto optimal design point is achieved with weight $w = 0.68$. Figure 7 shows the optimal flap configuration corresponding to the Pareto optimal design P.

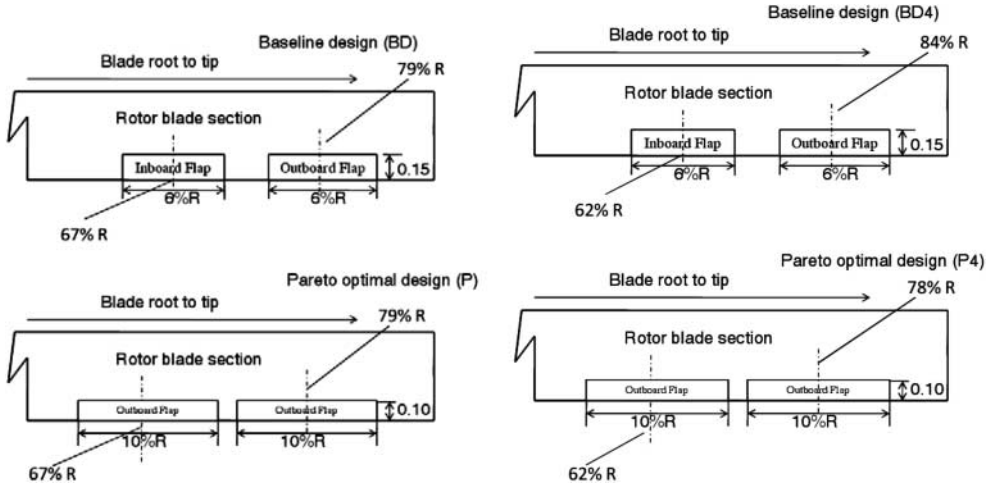


Figure 7. Schematic of rotor blade with optimal trailing edge flap configuration for two and four parameters.

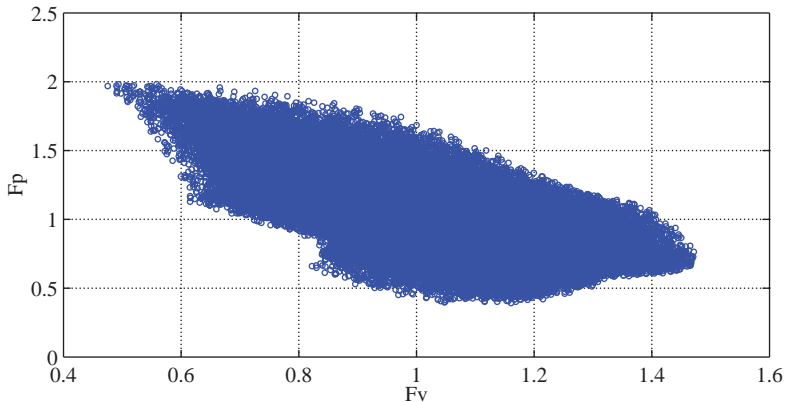


Figure 8. Objective space for dual flap configuration with four parameters.

Figure 8 shows the objective space for four parameters, inboard flap, outboard flap, flap length, and flap chord. Here, it is quite evident that the objective is non-convex for a partial region of interest. However, the MOBA algorithm is able to capture the necessary information to construct the Pareto curve as shown in Figure 9. In 4-parameter analysis, the minimum F_v and F_p design points are obtained only if the outboard flap is located near the tip, i.e. at $90\%R$, which is not recommended due to 3D aerodynamic effects and also it will demand high torque requirements due to large centrifugal forces. Therefore, the focus here is aimed at obtaining a more practical Pareto optimal configuration which simultaneously minimizes both the objectives. Pareto optimal point P4 represents a trade-off design for four parameters, which leads to the location of inboard and outboard flap midpoints at $62\%R$ and $78\%R$, respectively, while the Pareto optimal point P4 dictates using a flap length of $10\%R$ and a flap chord of $0.10c$, which is also inline with the results obtained from 2-parameter analysis. This confirms that the largest flap span and smallest flap chord will generate the optimal trade-off design. The design point P4 reduces vibration by 73% from the baseline (w/o flaps). Pareto optimal design P4 is also an improved design configuration relative to the baseline design point BD4, as it reduces vibratory loads by 14% and requires 27% less power for flap actuation than BD4. Figure 7 illustrates the optimal design configuration and locations for multiple trailing edge flaps for the 4-parameter case.

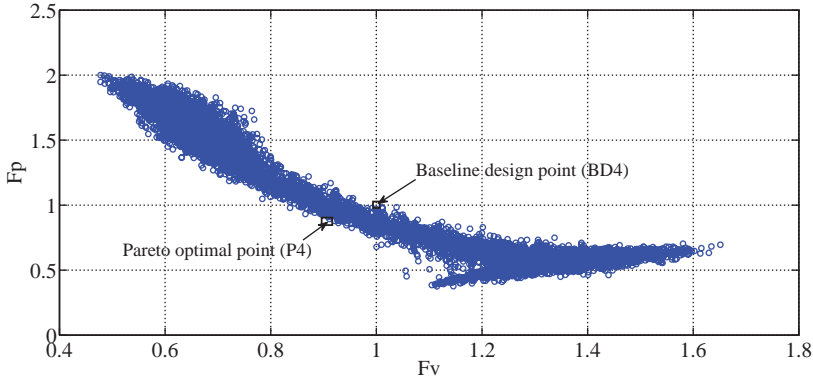


Figure 9. Pareto curve for dual flap configuration with four parameters.

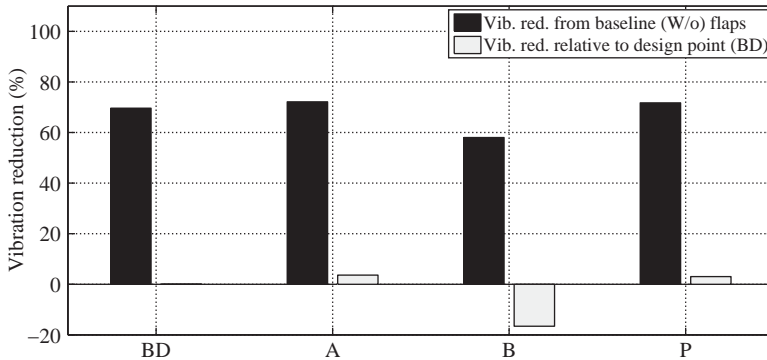


Figure 10. Vibration reduction from the baseline case (without flaps) for (a) baseline design point BD, (b) min. F_v design A, (c) min. F_p design B, and (d) Pareto optimal point P.

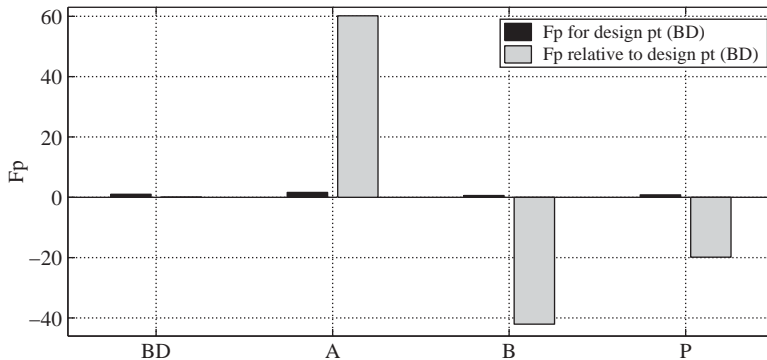


Figure 11. F_p for (a) Baseline design point BD (b) Min. F_v design (A) c) Min. F_p design (B) and (d) Pareto optimal point P.

Figures 10 and 11 show a detailed comparison of different objectives at design points S, A, B, and P for the 2-parameter case. Two interesting design points A and B are discovered along with Pareto optimal point P from the set of design points which collectively constitutes the Pareto front, as shown in Figure 6. Figures 12 and 13 show the hubloads and flap motion histories of the inboard and outboard flap for different design configurations, respectively. It is found that hubloads are minimum with flap configuration obtained with design point A. Figure 13 illustrates

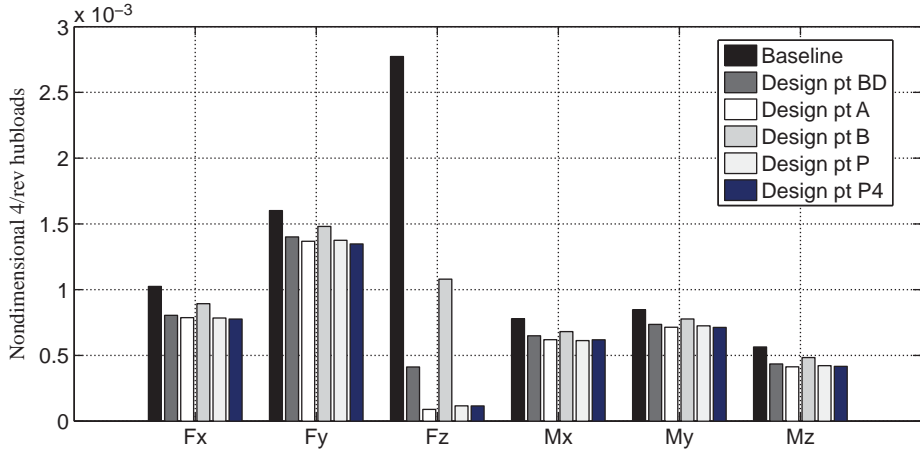


Figure 12. Hubloads with (a) Baseline design point BD (b) Min. F_v design A (c) Min. F_P design (B) (d) Pareto optimal point P and (e) Pareto optimal point P4.

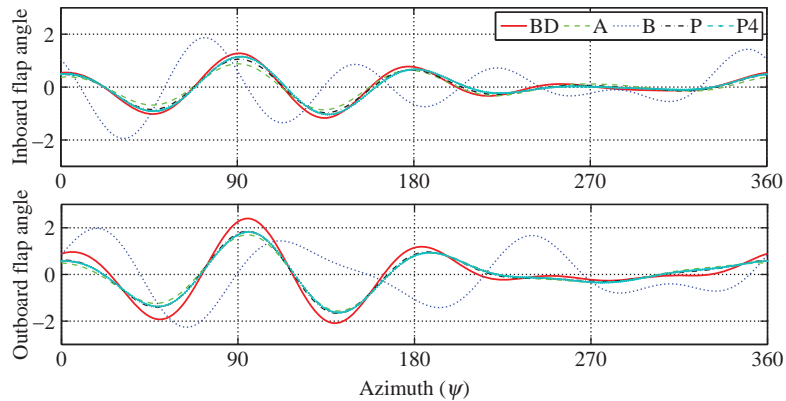


Figure 13. Inboard and outboard flap motion profiles at different design points.

that higher flap oscillations are required for design point B, and in particular the outboard flap has higher flap angles; this can be attributed to its higher dynamic pressure region working zone (Leishman, 2006). It is apparent that the flap configuration suggested by design point B could be an attractive choice for all practical purposes, as the flap power requirement is minimal along with a moderate reduction in the vibration levels. The Pareto optimal design points obtained from surrogate models using the multi-objective bat algorithm lead to finding a robust design which yields a substantial reduction in vibration levels and also reduces flap actuation power by around 40% in comparison with the minimum vibration design point A. Table 11 shows a sensitivity analysis for the 2-parameter case. Robustness of the optimal point is apparent from the fact that, with 1 and 2% perturbation in the design variables, the percentage vibration reduction from the baseline is still more than 70% and is quite close to the optimal value obtained for point P. Pareto design point P4 guides towards a marginal improvement over design point P in terms of overall vibration levels. Therefore, the optimal dual flap design configuration should have its inboard and outboard flaps midpoints positioned at 62% R and 78% R , respectively, with 10% R flap length and 0.10c flap chord. However, in terms of hub load reduction, both Pareto optimal points P and P4 have almost the same level of vibration reduction and flap oscillations, as is also evident from Figures 12 and 13.

Table 11. Sensitivity analysis for the 2-parameter case.

Sample point	x_1 (%R)	x_2	Percentage vibration reduction
1	10	0.10	72.83 (P)
2	10	0.09	71.58
3	9	0.09	70.88
4	10	0.08	71.38
5	8	0.08	70.02
6	10	0.12	71.93
7	10	0.11	71.56

9. Conclusions

In this investigation, a Pareto optimal dual flap configuration and locations are found which yield considerable reduction in hub vibration levels and require less flap actuation power. Cascading aeroelastic analysis with conventional optimization algorithms is a computationally expensive exercise. To address this problem, surrogate models are employed in this research. Two new 3-level design orthogonal arrays called MGB2P-OA and MGB4P-OA are proposed to develop second-order polynomial response surfaces with all interaction terms. A new metaheuristic evolutionary multi-objective bat algorithm is used to conduct optimization for optimal flap design. Two optimization problems are formulated and analysed, one with two parameters, flap chord, and flap length, and the other with four parameters, inboard flap position, outboard flap location, flap length, and flap chord, as design variables with the aim of simultaneously minimizing the hubloads and flap actuation power. Numerical results are obtained for a 4-bladed hingeless rotor system. Orthogonal array inspired polynomial response surfaces require fewer design experiments. The maximum variation in the response surface and aeroelastic prediction are around 6% for F_v and 4% for F_P . In this study, 3-level design OAs are adopted to create metamodels. Second-order polynomial response surfaces adequately approximate the hub vibration levels and flap actuation power, albeit higher level design OAs can be explored to reduce the residue further. However, there is a trade-off between the computational cost and the desired accuracy. The multi-objective bat algorithm leads to a Pareto front which yields two interesting design points A and B, along with a set of Pareto optimal points on the Pareto front for the 2-parameter case. A particular Pareto optimal design can be selected from this set on the basis of physical constraints and the requirements of the user. Pareto optimal design points P and P4 are obtained for the 2-parameter and 4-parameter cases, respectively, which yield substantial vibration reduction and require 20 and 27% less flap power than the baseline designs BD and BD4, respectively.

In the 2-parameter optimization problem, minimum hub vibration levels are obtained for design point A, which suggests using 10%R inboard and outboard flap lengths and a 0.15c flap chord ratio. However, a flap actuation power penalty is incurred for design point A, since larger flap dimensions require higher hinge moments. The minimum F_v design is found to be sensitive to the flap length. Minimum flap actuation power is obtained with design point B, which suggests deploying small flaps (4%R flap length and 0.10c flap chord). Design configuration B needs around 42% less flap actuation power in comparison to baseline design point BD. However, for the 4-parameter case, minimum F_v and F_P are obtained only if the outboard flap is positioned at 90%R, which is not suited for its higher dynamic pressure working zone. Therefore, focus is drawn towards the more practical Pareto optimal design. Therefore, the final optimal dual flap design configuration is characterized by inboard and outboard flap midpoints located at 62%R and 78%R, respectively, having 10%R flap span and 0.10c flap chord.

It can be inferred from this investigation that the second-order polynomial response surface inspired by the authors' newly proposed orthogonal arrays MGB2P-OA and MGB4P-OA can be used to construct accurate metamodels for complex and expensive aeroelastic problems. Design optimization for helicopters is a highly intricate phenomenon due to various conflicting objectives. Here, a multi-objective optimization algorithm such as the MOBA algorithm can serve as a useful tool to address complex helicopter design optimization problems to obtain robust optimal designs.

References

- Altringham, John D., Lucy Hammond, and Tom McOwat. 1996. *Bats: Biology and Behaviour*. Oxford, UK: Oxford University Press.
- Bhadra, Smita, and Ranjan Ganguli. 2006. "Aeroelastic Optimization of a Helicopter Rotor Using Orthogonal Array-Based Metamodels." *AIAA Journal* 44 (9): 1941–1951.
- Bir, Gunjit, Inderjit Chopra, K. C. Kim, J. Wang, E. Smith, S. Vellaichamy, R. Ganguli, M. Nixon, and S. Torok. 1992. "University of Maryland Advanced Rotorcraft Code (UMARC) Theory Manual." UM-Aero Report 92-02, University of Maryland, College Park, MD.
- Cesnik, C. E. S., D. G. Opoku, F. Nitzsche, and T. Cheng. 2004. "Active Twist Rotor Blade Modelling Using Particle-Wake Aerodynamics and Geometrically Exact Beam Structural Dynamics." *Journal of Fluids and Structures* 19 (5): 651–668.
- Chattopadhyay, Aditi. 1992. "Vibration Reduction in an Articulated Rotor Blade Using Structural Optimization." *Engineering Optimization* 19 (1): 37–50.
- Coello Coello, Carlos A. 1999. "An Updated Survey of Evolutionary Multiobjective Optimization Techniques: State of the Art and Future Trends." In *Proceedings of the 1999 Congress on Evolutionary Computation (CEC 99)*, 6–9 July 1999, Washington, DC, Vol. 1. Piscataway, NJ: IEEE. doi:10.1109/CEC.1999.781901.
- Crossley, William A., Valana L. Wells, and David H. Laananen. 1995. "The Potential of Genetic Algorithms for Conceptual Design of Rotor Systems." *Engineering Optimization* 24 (3): 221–238.
- Deb, Kalyanmoy. 2001. *Multi-Objective Optimization Using Evolutionary Algorithms*. Vol. 2012 of *Wiley-Interscience Series in Systems and Optimization*. Chichester, UK: Wiley.
- Fonseca, Carlos M., and Peter J. Fleming. 1995. "An Overview of Evolutionary Algorithms in Multiobjective Optimization." *Evolutionary Computation* 3 (1): 1–16.
- Friedmann, Peretz P., and Thomas A. Millott. 1995. "Vibration Reduction in Rotorcraft Using Active Control – a Comparison of Various Approaches." *Journal of Guidance, Control, and Dynamics* 18 (4): 664–673.
- Ganguli, R. 2002. "Optimum Design of a Helicopter Rotor for Low Vibration Using Aeroelastic Analysis and Response Surface Methods." *Journal of Sound and Vibration* 258 (2): 327–344.
- Ganguli, Ranjan. 2004. "A Survey of Recent Developments in Rotorcraft Design Optimization." *Journal of Aircraft* 41 (3): 493–510.
- Ganguli, Ranjan. 2012. *Engineering Optimization: A Modern Approach*. Hyderabad: Universities Press.
- Geem, Zong Woo. 2009. "Multiobjective Optimization of Time–Cost Trade-Off Using Harmony Search." *Journal of Construction Engineering and Management* 136 (6): 711–716.
- Glaz, Bryan, Tushar Goel, Li Liu, Peretz P. Friedmann, and Raphael T. Haftka. 2009. "Multiple-Surrogate Approach to Helicopter Rotor Blade Vibration Reduction." *AIAA Journal* 47 (1): 271–282.
- Hariharan, Nagarajan, and J. Gordon Leishman. 1996. "Unsteady Aerodynamics of a Flapped Airfoil in Subsonic Flow by Indicial Concepts." *Journal of Aircraft* 33 (5): 855–868.
- Hasançebi, O., T. Teke, and O. Pekcan. 2013. "A Bat-Inspired Algorithm for Structural Optimization." *Computers & Structures* 128:77–90.
- Hu, Yi, and Singiresu S. Rao. 2011. "Robust Design of Horizontal Axis Wind Turbines Using Taguchi Method." *Journal of Mechanical Design* 133 (11), Paper No. 111009. doi:10.1115/1.4004989.
- Johnson, Wayne. 1982. "Self-Tuning Regulators for Multicyclic Control of Helicopter Vibration." NASA Technical Paper 1996. <http://ntrs.nasa.gov/archive/nasa/casi.ntrs.nasa.gov/19820012314.pdf>.
- Konstanzer, Peter, Bernhard Enenkl, P. Aubourg, and P. Cranga. 2008. "Recent Advances in Eurocopter's Passive and Active Vibration Control." In *Proceedings of the 64th AHS Annual Forum of the American Helicopter Society*, 29 April–1 May 2008, Montreal, Quebec, Canada, Vol. 1, 424–441. Alexandria, VA: American Helicopter Society.
- Leishman, J. Gordon. 2006. *Principles of Helicopter Aerodynamics*. New York: Cambridge University Press.
- Lim, In-Gyu, and In Lee. 2009. "Aeroelastic Analysis of Rotor Systems Using Trailing Edge Flaps." *Journal of Sound and Vibration* 321 (3): 525–536.
- Loewy, Robert G. 1984. "Helicopter Vibrations – a Technological Perspective." *Journal of the American Helicopter Society* 29 (4):4–30.
- Mallick, Rajnish, Ranjan Ganguli, and M. Seetharama Bhat. 2013. "Robust Design of Trailing Edge Flap with Orthogonal Array Inspired Response Surface for Helicopter Vibration Reduction." In *Proceedings of the 39th European Rotorcraft Forum*, 3–6 September 2013, Moscow. Moscow: Russian Helicopters, JSC.

- Mallick, Rajnish, Ranjan Ganguli, and M. Seetharama Bhat. 2014. "An Experimental and Numerical Study of Piezoelectric Actuator Hysteresis in Helicopter Active Vibration Control." *Proceedings of the Institution of Mechanical Engineers, Part G: Journal of Aerospace Engineering* 228 (5): 690–705.
- Milgram, Judah, Inderjit Chopra, and Friedrich Straub. 1998. "Rotors with Trailing Edge Flaps: Analysis and Comparison with Experimental Data." *Journal of the American Helicopter Society* 43 (4): 319–332.
- Murugan, M. S., R. Ganguli, and D. Harursampath. 2012. "Surrogate Based Design Optimisation of Composite Aerofoil Cross-Section for Helicopter Vibration Reduction." *Aeronautical Journal* 116 (1181): 709–725.
- Myers, Raymond H., Douglas C. Montgomery, and Christine M. Anderson-Cook. 2011. *Response Surface Methodology: Process and Product Optimization Using Designed Experiments*. 3rd ed. Vol. 705 of Wiley Series in Probability and Statistics. Hoboken, NJ: Wiley.
- Noboru, Kobiki, Shigeru Saito, Takehito Fukami, and Takayoshi Komura. 2007. "Design and Performance Evaluation of Full Scale On-Board Active Flap System." In *Proceedings of the 63rd AHS Annual Forum of the American Helicopter Society*, 1–3 May 2007, Virginia Beach, VA, 707–717. Alexandria, VA: American Helicopter Society.
- Pearson, J. T., R. M. Goodall, and I. Lyndon. 1994. "Active Control of Helicopter Vibration." *Computing & Control Engineering Journal* 5 (6): 277–284.
- Rao, S. S., A. K. Dhingra, and H. Miura. 1990. "Pareto-Optimal Solutions in Helicopter Design Problems." *Engineering Optimization* 15 (3): 211–231.
- Richardson, Phil. 2011. *Bats*. Revised and reformed. New York: The Natural History Museum.
- Roy, Ranjit K. 2010. *A Primer on the Taguchi Method*. 2nd ed. Dearborn, MI: Society of Manufacturing Engineers.
- Shen, Jinwei, and Inderjit Chopra. 2004. "A Parametric Design Study for a Swashplateless Helicopter Rotor with Trailing-Edge Flaps." *Journal of the American Helicopter Society* 49 (1): 43–53.
- Simpson, Timothy W., J. D. Poplinski, Patrick N. Koch, and Janet K. Allen. 2001. "Metamodels for Computer-Based Engineering Design: Survey and Recommendations." *Engineering with Computers* 17 (2): 129–150.
- Sinapius, Michael, Hans Peter Monner, Markus Kintscher, and Johannes Riemenschneider. 2014. "DLR's Morphing Wing Activities within the European Network." *Procedia IUTAM* 10: 416–426.
- Sobiesczanski-Sobieski, Jaroslaw, and Raphael T. Haftka. 1997. "Multidisciplinary Aerospace Design Optimization: Survey of Recent Developments." *Structural Optimization* 14 (1): 1–23.
- Viswamurthy, S. R., and Ranjan Ganguli. 2007. "Optimal Placement of Trailing-Edge Flaps for Helicopter Vibration Reduction Using Response Surface Methods." *Engineering Optimization* 39 (2): 185–202.
- Wilke, Gunther. 2013. "Multi-Objective Optimizations in Rotor Aerodynamics Using Variable Fidelity Simulations." In *Proceedings of the 39th European Rotorcraft Forum*, 3–6 September 2013, Moscow. Moscow: Russian Helicopters, JSC.
- Yang, Xin-She. 2011a. "Bat Algorithm for Multi-Objective Optimisation." *International Journal of Bio-Inspired Computation* 3 (5): 267–274.
- Yang, Xin-She. 2011b. "Review of Meta-Heuristics and Generalised Evolutionary Walk Algorithm." *International Journal of Bio-Inspired Computation* 3 (2): 77–84.
- Yang, Xin-She, and Amir Hossein Gandomi. 2012. "Bat Algorithm: A Novel Approach for Global Engineering Optimization." *Engineering Computations* 29 (5): 464–483.
- Yang, Xin-She, and Xingshi He. 2013. "Bat Algorithm: Literature Review and Applications." *International Journal of Bio-Inspired Computation* 5 (3): 141–149.